Occluded cobalt species over ZSM-5 matrix: design, preparation, characterization and magnetic behavior

Liliana B. Pierella[1,3*], Clara Saux[1,3], Héctor R. Bertorello[2,3], Paula G. Bercoff [2,3] , Pablo M. Botta[4], J. Rivas[4]

[1] Grupo Zeolitas - CITeQ (Centro de Investigación y Tecnología Química), Facultad Córdoba, Universidad Tecnológica Nacional. 5016- Córdoba-Argentina. Tel-FAX: 54-351-4690585- Email: lpierella@scdt.frc.utn.edu.ar

[2] Facultad de Matemática, Astronomía y Física, Universidad Nacional de Córdoba. Córdoba-Argentina.

[3] Conicet (Consejo Nacional de Investigaciones Científicas y Técnicas), Argentina.

[4] Departamento de Física Aplicada, Universidad de Santiago de Compostela, Facultad de Física, Campus Sur, 15782 Santiago de Compostela, Spain.

Abstract

Co-containing molecular sieve with MFI structure was synthesized by the hydrothermal crystallization method and cobalt was incorporated in it by wet impregnation at different percentages. Thermal post-treatments were applied to Co-ZSM-5: calcination and reduction. XRD and FTIR analysis confirmed crystallinity, structure and orthorhombic symmetry of the obtained samples (Co-ZSM-5 calcined and Co-ZSM-5 reduced). The XRD, Raman Spectroscopy, SEM and TPR techniques for the calcined samples showed the presence of Co_3O_4 which diminished in the reduced samples and new cobalt species appeared (CoO and Co^0). The magnetic behavior of the materials was evaluated by magnetization (*M*) variation with applied magnetic field (*H*)

at room temperature. Low magnetization is observed in the calcined samples while high values are attained in the reduced samples, due to the presence of metallic Co.

Keywords: A. Microporous Materials; D. Magnetic Properties

*****To whom correspondence should be addressed

1. Introduction

Micro and nanoparticles can often display properties that differ from their bulk counter-part. At the same time, they can be adapted or modified for different applications by adding dopants to the lattice or adding small particles clusters of elements or oxides to a determined kind of matrix.

The investigation of the properties of magnetic ultrafine particle systems has attracted a lot of attention during the last two decades because of the continuous increase of the number of applications of new magnetic materials [1, 2]. When the size of magnetic particles is reduced to a few tens of nano and micrometers, they exhibit a number of outstanding physical properties such us giant magnetoresistence (GMR), superparamagnetism, large coercivities, high Curie temperature and high saturation magnetization as compared to the corresponding bulk values [1, 3-5]. The synthesis of magnetic systems with characteristic sub-nano, nano and microscale dimensions has attracted a lot of research attention. The production of heterogeneous magnetic materials with controlled and reproducible composition and structure is a great challenge. The deposition of small particles of magnetic materials, anchoring or doping as isolated aggregates, over diverse supports is extensively studied [6-8]. However, Co-ZSM-5

magnetic properties have not been investigated enough. To our knowledge, only Corma *et al*. [9] have published some results on Co-zeolites with Co located in the framework.

Magnetic ultrafine particles can be widely used in many important areas of high technology such as ferrofluids, catalysts, ultra-high density magnetic storage media, biomedical and medical treatments and analyses, high-frequency soft magnetic materials, and microwave absorbing materials [10]. Some materials such as titanium oxide loaded with other transition metals (Co, Fe, Mn, Ni) can be potentially used in a wide range of applications (optical, opto-electronics, magnetism and many other developments) [11, 12], as well as the catalysis area (photocatalysis) [13, 14].

On the other hand, it is essential that the matrixes used as transition metal supports have high cristallinity, purity, great stability and small particles size.

Zeolites and related microporous molecular sieves consist of a three-dimensional network of metal-oxygen tetrahedra (in a few cases also octahedra) which provide the microporous-sized periodic structure, where the active sites are present. Active sites (generally acid sites) result from the imbalance of the metal and the oxygen formal charge in the primary building unit (crystalline aluminosilicates) [15, 16]. These materials with well defined pores, channels and/or cavities are well known for their shape selectivity properties as well as for their catalytic properties on several technological processes and high deactivation/mechanic resistance [15, 17].

ZSM-5 (MFI type structure: Mirror Framework Inversion) pentasyl zeolites with 5.1-5.6 Å pore diameter (classified as microporous aluminosilicate systems with orthorhombic symmetry) and well defined tubular channels, offer enough space inside their channels and over the external crystal surface for localization of cations with

different oxidation state, according to the method employed in the matrix loading, to the thermal post-treatments applied and to the cation incorporation percentage [18].

Co-ZSM-5 and Cu-ZSM-5 zeolites were effective on NO_x selective reduction process (SCR) [19-22]. Co-MFI zeolite showed better hydrothermal stability than Cu-MFI [23], so Co-zeolite has been extensively studied in many developments and investigation groups [24-26]. Co-MFI applications on alkenes and alkilaromatics autoxidation were also informed [27].

Recently, we reported the magnetic properties of cobalt-hosted zeolites with MFI matrix, where cobalt cations were incorporated by the ion-exchange technique and in different concentrations than the samples studied in this work [28]. In this work we report the preparation and characterization of a Co-microporous zeolite matrix with MFI structure by wet impregnation. As a first approximation, we discuss the structural characteristics of the obtained materials and their connection to the magnetic properties.

2. Experimental

Materials preparation

ZSM-5 material (Si/Al=17) was obtained by the hydrothermal crystallization method. Aqueous solution of sodium aluminate was introduced into a Si_2O solution which was prepared previously by partial dissolution on tetrapropylammonium hydroxide (TPAOH) aqueous solution. The obtained gel reached a pH > 9 and was maintained at 393-433 K for 12-16 days under self-generated pressure on autoclave. Afterwards, reaction products were extracted, washed and dried at 383 K for 12 h. The structure directing agent (TPA) was desorbed in N_2 atmosphere (20 ml/min) at programmed temperature (10 K/min) from 383 K to 793 K and then it was calcined in

air at 793 K for 12 h to obtain Na-ZSM-5. The ammonium form of the material (NH_4-zeolite) was prepared by ion-exchange with NH_4Cl (1 M) for 40 h at 353 K from Na-zeolite [29].

Co-ZSM-5 samples were produced using the porous material (NH_4-ZSM-5 zeolite) with a surface area of 389 m^2/g, and were impregnated by the solution of $CoCl_2.6H_20$, until reaching the desired cation content. After that, the samples were dried at 383 K and desorbed in N_2 flow (10 ml/min) at programmed temperature (10 K/min) from 383 K to 773 K for 12 h followed by calcination in air at 773 K for 12 h. The final product was denominated Calcined Co-ZSM-5 zeolite (CoxIC where x = Co wt %).

Calcined Co-samples were reduced under an H_2 flow (10 ml/min), from room temperature to 773 K at 5 K/min, keeping constant this final temperature for 5 h. The final product was denominated Reduced Co-ZSM-5 zeolite (CoxIR where x = Co wt %).

Materials characterization

The MFI structure pentasyl materials modified with Co cations were characterized by different techniques.

In order to determine the exact content of Co in the prepared materials, Atomic Absorption analyses were carried out using a Perkin Elmer Analyst 800 spectrometer after the digestion of the samples by microwave in a Milestone ETHOS 900 digester.

BET surface area determinations were carried out with ASAP 2000 equipment.

X ray diffraction (XRD) patterns were performed in a Philips diffractometer using CuKα radiation. The patterns were taken between 2θ=30º and 70º with a step of 0.02º.

Raman spectra were obtained at room temperature with a Renishaw Dispersive 1000 system, equipped with a cooled TCD and holographic Notch filter.

Temperature programmed reduction (TPR) experiments were performed on an Okhura TP 2002 S instrument equipped with a TCD detector. The reducing gas system was 5% H_2 on Ar, at 30 ml/min and heating rate of 10 K/min from room temperature to 1173 K.

Infrared (IR) analyses of Co-zeolites were performed on a JASCO 5300 FTIR spectrometer. The spectra in the lattice vibration region were performed using KBr 0.05% wafer technique and they were carried out from 1800-400 cm^{-1} in 16 consecutive registers of 4 cm^{-1} resolution each one.

A LEO 1450 VP Scanning Electron Microscope (SEM) was used to take the micrographs and an energy dispersive system (EDS) spectrometer Genesis 2000 was used to perform a qualitative electron probe microanalysis (EPMA). The SEM micrographs and EDS spectra were taken with an incident electron beam of 20 keV. In order to prepare the samples, the powders were dusted on a carbon adhesive tab placed on an aluminum stub and carbon or gold coated. The micrographs were taken using backscattered electrons (BSE) which mainly give information of chemical contrast, as the BSE intensity is strongly dependant on the mean atomic number of the sample. The results were confirmed by EPMA.

Magnetic measurements were performed on the samples at room temperature using a Vibrating Sample Magnetometer Lakeshore 7300 which can reach a maximum magnetic field of 15 kOe. The powders were shaped into disks of 6 mm diameter and 1 mm height using an organic binder and compacted with the aid of a uniaxial press. For

measurements at different temperatures a commercial superconducting quantum interference device (SQUID) was used, varying the applied field up to 20 kOe.

3. Results and Discussion

According with BET results the MFI zeolite showed a 382 m^2/g of surface area. The analyses performed by Atomic Absorption revealed that a 2.8 Co wt% was effectively incorporated for sample Co2.8I and a 4.9 Co wt% for sample Co4.9I, respectively. XRD and FTIR (on the fingerprint zone) results showed 98% and 97% of crystallinity for both cobalt samples. Structure and orthorhombic symmetry were confirmed.

Figures 1 and 2 illustrate the XRD patterns of Co-zeolites between $2\theta = 30$ and 70º, where the majority of the peaks correspond to the matrix. Cobalt oxides and metal Co signals are observed. In the spectra corresponding to the calcined samples the presence of CoO and Co_3O_4 is also noticed. This phase is particularly notorious in sample Co4.9IC. In the reduced samples the proportion of oxides is considerably lower (as expected) and the presence of metallic Co is detected in a cubic phase, as well as traces of hexagonal Co. However, the oxides were not completely reduced, as some peaks corresponding to CoO and Co_3O_4 are still present.

Figure 1

Figure 2

From SEM micrographs and EPMA spectra we can infer that the bright spots seen on the external surface of the particles correspond to Co oxide in both calcined samples (high peaks at 6.955 keV and 7.649 keV, the characteristic energies of Co Kα and Kβ respectively, and 0.775 and 0.79 keV, the characteristic energies of Co Lα and

Lβ respectively). The higher Co content in sample Co4.9IC is evident from the larger number of bright spots in Figure 4 with respect to Co2.8IC (Figure 3). The size of these particles is about 2 μm and they are evenly distributed over the surface of the zeolite. This technique is not capable of giving accurate information on the species contained inside the channels of the structure, but according to EPMA diagrams performed far from a bright spot in both samples there is a small contribution of Co which would indicate the presence of this element inside the matrix. Figures 3 and 4 led us to get an insight into the presence and distribution of the Co oxides on the external surface of the zeolite particles. Smaller (nanometric) Co particles could also be present on the surface of the zeolite, but the magnification of the microscope was not large enough to detect them.

Figure 3

Figure 4

The TPR profiles of samples Co2.8IC and Co2.8IR; Co4.9IC and Co4.9IR are shown in Figure 5.

In order to compare the studied samples, it is necessary to consider the influence of some parameters which affect or modify a Programmed Temperature Profile, such as heating rate, gas flow and concentration, particle size, mass to reduce, percentage of reducible substances, and others.

In the case of the calcined materials, the reduction profile was induced in two steps. The lower temperature signal of the TPR profile (573-773 K) can be assigned to the two-step reduction of Co_3O_4 (with minimal support interaction) to CoO and then to Co^0 [30]. The second signal (773-1080 K) could be tentatively assigned to the

reduction of a small part of Co^{2+} located at exchange positions or some small Co_xO_y clusters having a relatively stronger interaction with the framework [31-33].

Figure 5

The TPR profiles of the reduced samples (Co2.8IR and Co4.9IR) also presented two important H_2 consumption regions. The first great band at low temperatures (423-653 K), of less intensity than the corresponding to the calcined samples showed that even after the reduction treatment, some species related to non-reduced oxide phases were still present and they could be reduced with this new reduction treatment. This is consistent with the results obtained by XRD.

This behavior could also be associated to not adequate reduction conditions (H_2 flow, time on stream, temperature, etc) employed to reach the complete reduction of Co_3O_4, (the main oxide phase present on the calcined sample) and CoO (found in less proportion), according to XRD results observed in Figures 1 and 2. The XRD patterns of the reduced samples showed an important intensity decrease of the oxide signal and peaks that correspond to metallic cubic cobalt as well as traces of hexagonal Co appeared. The second H_2 consumption band (700-1080 K) on the TPR profiles could be related with an incomplete reduction produced by an insufficient treatment for the species with the highest reduction temperature, which have a relatively strong interaction with the framework [19, 31, 32].

As shown in Figure 5, the reduction bands are shifted to lower temperatures in samples Co4.9IR, Co2.8IC and Co2.8IR, in which the content of the cobalt oxide species is considerably decreased. This behavior is more evident in the previously reduced samples (Co4.9IR and Co2.8IR). Even when H_2 concentration in the gas flow was kept constant at all the experiments (5% H_2 in Ar, 30 ml/min), the

hydrogen/reducible-species ratio was decreased in the sample with more Co content (Co4.9IC) resulting in a lower reduction rate and shifting the TPR profile to higher temperatures.

According to Raman spectroscopy results for the calcined materials (Figure 6), cobalt species on the 450-700 cm^{-1} zone [33, 34] and a wide band near 375 cm^{-1} -which is characteristic from ZSM-5 zeolite structure [32, 35, 36]- were observed. Bands at 675-694, 510-528 and 450-488 cm^{-1} are typical of microcrystalline Co_3O_4 (cobalt oxide spinel phase) [34]. This phase coexists with exchanged Co ions which are the responsible for the signals that appeared at 600-630 cm^{-1}. However, it should be remarked that Raman Spectroscopy does not give enough information about Co^{2+}species at exchange positions. Raman bands for Co_3O_4 were considerably weaker in the reduced samples (see the inset of Figure 6) because of its reduction to CoO and Co metal.

Figure 6

According to magnetization measurements performed at T=10 K, the maximum magnetization at a field of 20 kOe measured for both of the calcined samples is about 30 emu/gCo. In both cases the main observed behavior is paramagnetic, as shown by the slope of the curves, which do not saturate. Figure 7 shows the curves M vs H (first quadrant) at different temperatures for sample Co4.9IC. The analogous curves for sample Co2.8IC are almost identical to these and are not shown. The fact that the maximum magnetization is almost the same for both samples −Co2.8IC and Co4.9IC− despite the last one has a higher Co content, would indicate that the Co inside the zeolite structure is present as an oxide with paramagnetic behavior and the Co excess is located at the surface of the zeolite particles, in the form of oxides with no magnetic

contribution. This is consistent with the results obtained by XRD for these samples. At the moment we can not infer what kind of Co species are present inside the zeolite structure but they are presumably in the form of small clusters due to the small volume available inside the channels of the zeolite. Those clusters would have a superparamagnetic behavior like the one observed in samples where Co species were introduced via ionic exchange [28]. Table 1 contains the values of the maximum magnetization at 20 kOe and the susceptibilies χ of the calcined samples, at different temperatures.

Table 1

Figure 7

Both M_{max} and χ decrease with increasing temperature for Co2.8IC and Co4.9IC.

After reducing in H_2, the magnetic behavior of both samples changes drastically. Figure 8 shows the M vs H curves (first quadrant) measured at different temperatures for sample Co4.9IR. The corresponding curves for sample Co2.8IR are very similar to the ones shown here, but with lower values of maximum magnetization, probably due to the reduced Co content. Ferromagnetic loops were obtained for all the temperatures. The values of maximum magnetization at 20 kOe and the coercivities, Hc, are given in Table 2 for both samples at different temperatures.

Figure 8

Table 2

The high values of M_{max} are assigned to cubic Co because it is the main ferromagnetic component observed by XRD in these samples. Its saturation magnetization at 0K is 166.1 emu/g [37]. Hexagonal Co only appears in low concentration and no other ferromagnetic phase is present in these samples. As T

decreases the maximum magnetization increases. The coercivity shows an increasing behavior with increasing T from 5K to 40K and then it decreases. The maximum in Hc at 40 K could be attributed to the appearance of magnetic contributions of ferromagnetic clusters, with blocking temperatures between 5K and 40K. When increasing the temperature beyond 40K the coercivity decreases with the temperature, as expected [38]. Sample Co4.9IR has lower coercivities than sample Co2.8IR at every measured temperature. This would indicate that the magnetic contribution comes from bigger particles in sample Co4.9IR, as the observed particles are big enough to be multidomain, and they follow the well-known behavior of decreasing coercivity with increasing domain size [38].

4. Conclusions

Through this study, we have been able to identify some of the cobalt species present in Co-ZSM-5 calcined and reduced materials as well as their correlation with the magnetic behavior. After calcinations, Co-zeolites contain Co_3O_4, Co_xO_y, and Co^{2+} located at exchange positions. After reducing, CoO, cubic Co and −in a lesser amount− hexagonal Co appear while the amount of Co_3O_4 decreases. The calcined samples have low magnetization at room temperature, as only antiferromagnetic oxides are present. In contrast, the reduced samples display large magnetization values, which correlate with the presence of micrometric Co particles, mainly cubic cobalt. An extensive study of the magnetic properties as a function of temperature and applied field is being conducted.

Acknowledgements

This project was supported partially by: CONICET-PIP N° 6313/05 and 6394/05, FONCYT-ANPCyT-PICT N° 14-14485/03 UTN-PID 25E092 and MAT2004-05130-C02-01 (MEC, Spain). We thank CONICET: L.B. Pierella, H.R. Bertorello and P.G. Bercoff (researchers); UTN: C. Saux (doctoral fellowship); P.M. Botta (researcher, program J. de la Cierva, MEC).

References

[1] D. Kumar, J. Narayan, A. Kvit, A. Sharma, J. Sankar, J. Magn. Magn. Mater. 232 (2001) 161

[2] N. Bagrets, N. Perou, A. Bagrets, A. Lermontou, G. Pankina, P. Chernavskii, J. Magn. Magn. Mater. 272 (2004) 1565

[3] J. Yu, U. Rudiger, L. Thomas, S. Parkin, A. Kent, J. Appl. Phys. 85 (1999) 5501

[4] A. Fidniki, C. Dorien, F. Richomme, J. Teillet, D. Lemarchand, N. Duc, J. Ben Youssef, H. Le Gall, J. Magn. Magn. Mater. 262 (2003) 368

[5] C. Chen, O. Kitakami, Y. Shimada, J. Appl. Phys. 84 (1998) 2184

[6] I. Park, M. Yoon, Y.M. Kim, Y. Kim, H. Yoon, H. Song, V. Volkov, A. Avilov, Y. Park, Solid State Commun. 44 (2003) 385

[7] S. Sun, C. Murray, D. Weller, L. Folks, A. Moser, Science 287 (2000) 1989

[8] J. Bansmann, S. Baker, C. Binns, J. Blackman, J. Bucher, J. Dorantes-Dávila, V. Dupuis, L. Favre, D. Kechrakos, A. Kleibert, K. Meiwes-Broer, G. Pastor, A. Perez, O. Toulemonde, K. Trohidou, J. Tuaillon, Y. Xie, Surf. Sci. Reports 56 (2005) 189

[9] E. Barea, V. Fornés, A. Corma, P. Bourges, E. Guillon and V. Puentes, Chem. Comm. (2004), 1974

[10] X. Lu, G. Liang, Z. Sun, W. Zhang, Mater. Sci. Eng. B 117 (2005) 147

[11] Y. Shen, H. Deng, J. Fang, Z. Lu, Colloids Surf. A 175 (2000) 135

[12] K. Gurunathan, D. Trivedi, Mater. Lett. 45 (2000) 262

[13] S. Sakthivel, M. Hidalgo, D. Bahnemann, S. Geissen, V. Murugesan, A. Vogelpohl, Appl. Catal. B: 63 (2006) 31

[14] N. Mahmoodi, M. Arami, N. Limaee, N. Tabrizi, J. Colloid Interface Sci. 295 (2006) 159

[15] M. Stocker, Micropor. Mesopor. Mater. 82 (2005) 257

[16] J.A. Lercher, A. Jentys, in: F. Schuth, K.S.W. Sing, J. Weitkamp (Eds.), Handbook of Porous Solids, Wiley-VCH, Weinheim, (2002) 1097

[17] P.B. Weisz, V.J. Frilette, J. Phys. Chem. 64 (1960) 382

[18] W.M. Meier, D.H. Olson, Atlas of Zeolite Structure Types, Butterworth-Heinemann, USA, (1992)

[19] X. Wang, H. Chen, M. Sachtler, Appl. Catal. B 26 (2000) L227

[20] J. Armor, Catal. Today 26 (1995) 107

[21] X. Wang, H. Chen, M. Sachtler, Appl. Catal. B 29 (2001) 47

[22] J. Miller, E. Glusker, R. Peddi, T. Zheng, J. Regalbuto, Catal. Lett. 51 (1998) 15

[23] V. Parvulescu, P. Grange, B. Delmon, Catal. Today 46 (1998) 233

[24] A. Stakheev, C. Lee, S. Park, P. Chong, Catal. Lett. 38 (1996) 271

[25] Y.G. Kim, Y.C. Kim, S. Hong, M. Kim, Y. Kim, Y. Uh, Catal. Lett 57 (1999) 179

[26] F. Geobaldo, B. Onida, P. Rivolo, F. Di Renzo, F. Fajula, E. Garrone, Catal. Today 70 (2001) 107

[27] I. Arends, R. Sheldon, Appl. Catal. A 212 (2001) 175

[28] H. Bertorello, L. Pierella, P. Bercoff, C. Saux, J. Sinnecker, Physica B 354 (2004) 137

[29] L.B. Pierella, Doctoral Tesis, Universidad Nacional de Córdoba (2000)

[30] B. Jongsomjit, J. Panpranot, J.G. Goodwin, J. Catal. 204 (2001) 98

[31] B. Jongsomjit, J. Goodwin Jr., Catal. Today 77 (2002) 195

[32] Q. Tang, Q. Zhang, H. Wu, Y. Wang, J. Catal. 230 (2005) 384

[33] A. Boix, E. Miro, E. Lombardo, M. Bañanes, R. Mariscal, J. Fierro, J. Catal. 217 (2003) 186

[34] H. Ohtsuka, T. Tabata, O. Okada, L. Sabatino, G. Bellussi, Catal. Lett. 44 (1997) 265

[35] P. Knops-Gerrits, D. De Vos, E. Feijen, P. Jacobs, Micropor. Mater. 8 (1997) 3

[36] Y. Yu, G. Xiong, C. Li, F.S. Xiao, Micropor. Mesopor. Mater. 46 (2001) 23

[37] R. M. Bozorth, "Ferromagnetism". IEEE Press, New York, 1993

[38] B. D. Cullity, Introduction to Magnetic Materials, Addison Wesley, Reading, MA, 1972. Section 11.6

Table 1: Maximum magnetization at 20 kOe and susceptibility χ for the calcined samples.

T [K]	M_{max} (20kOe) [emu/gCo]		χ [x 10^{-4} emu/(gCo Oe)]	
	Co2.8IC	**Co4.9IC**	**Co2.8IC**	**Co4.9IC**
10	30.3	30.6	15.60	15.50
40	9.2	10.1	4.70	5.10
120	3.1	3.8	1.60	1.90
300	2.1*	2.6*	0.65	0.76

**measured at 15 kOe, extrapolated to 20 kOe.*

Table 2: Maximum magnetization at 20 kOe and coercivity H_c for the reduced samples.

T [K]	M_{max} (20 kOe) [emu/gCo]		H_c [Oe)]	
	Co2.8IR	**Co4.9IR**	**Co2.8IR**	**Co4.9IR**
5	135.3	163.6	328	270
10	105.0	142.7	370	280
40	90.3	109.4	541	305
155	63.7	99.6	410	223
300	60.3*	93.1*	288	190

**measured at 15 kOe, extrapolated to 20 kOe.*

Figure captions

Figure 1: Diffraction patterns of samples Co2.8IC and Co2.8IR.

Figure 2: Diffraction patterns of samples Co4.9IC and Co4.9IR.

Figure 3: Micrography of Co2.8IC taken at 1500x. The bright spots are Co oxide particles.

Figure 4: Micrography of Co4.9IC taken at 1500x. The bright spots are Co oxide particles.

Figure 5: TPR profiles of Co2.8IC, Co2.8IR, Co4.9IC and Co4.9IR.

Figure 6: Laser Raman spectra of calcined Co2.8IC and Co4.9IC. Inset: Co2.8IC and Co2.8IR Laser Raman spectra.

Figure 7: *M vs H* curves for sample Co4.9IC at different temperatures.

Figure 8: *M vs H* curves for sample Co4.9IR at different temperatures.

Figure 1:

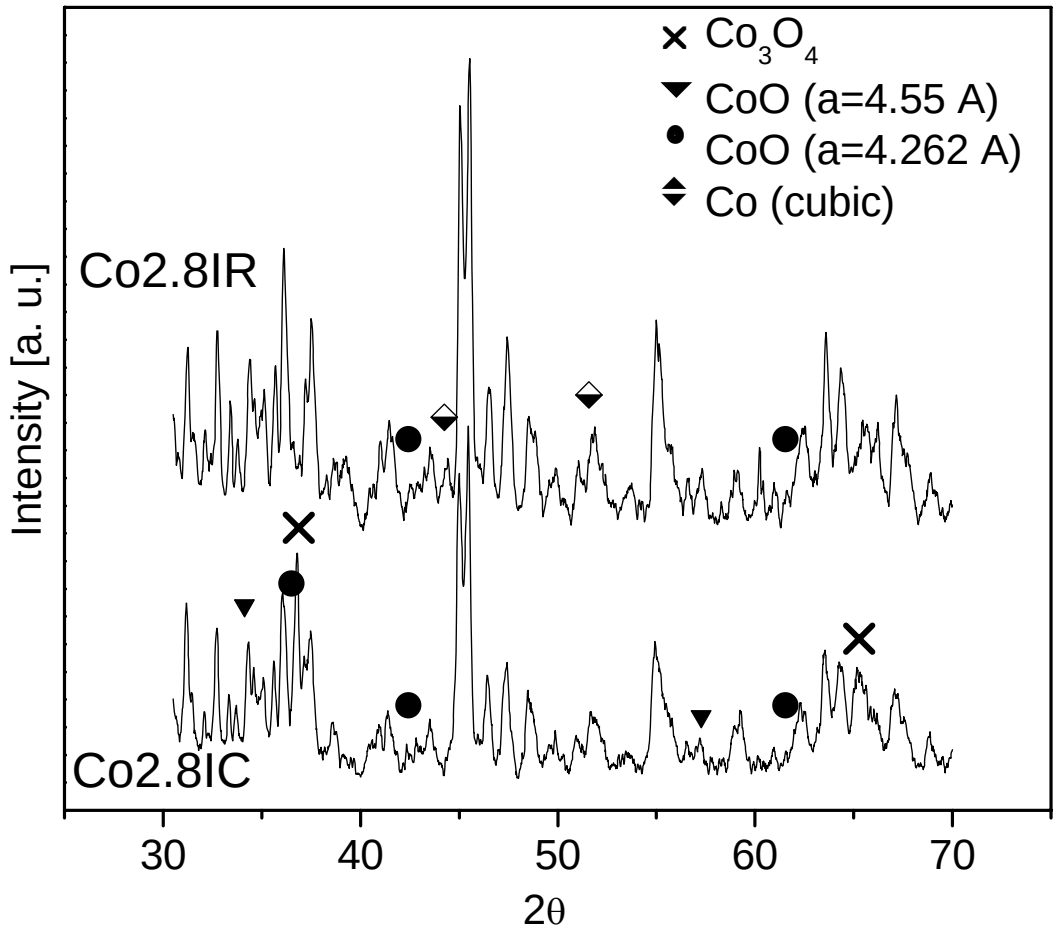
Co3O4
CoO (a=4.55 A)
CoO (a=4.262 A)
Co (cubic)
Co2.8IR
Co2.8IC
Intensity [a. u.]
30
40
50
60
70
2θ

Figure 2

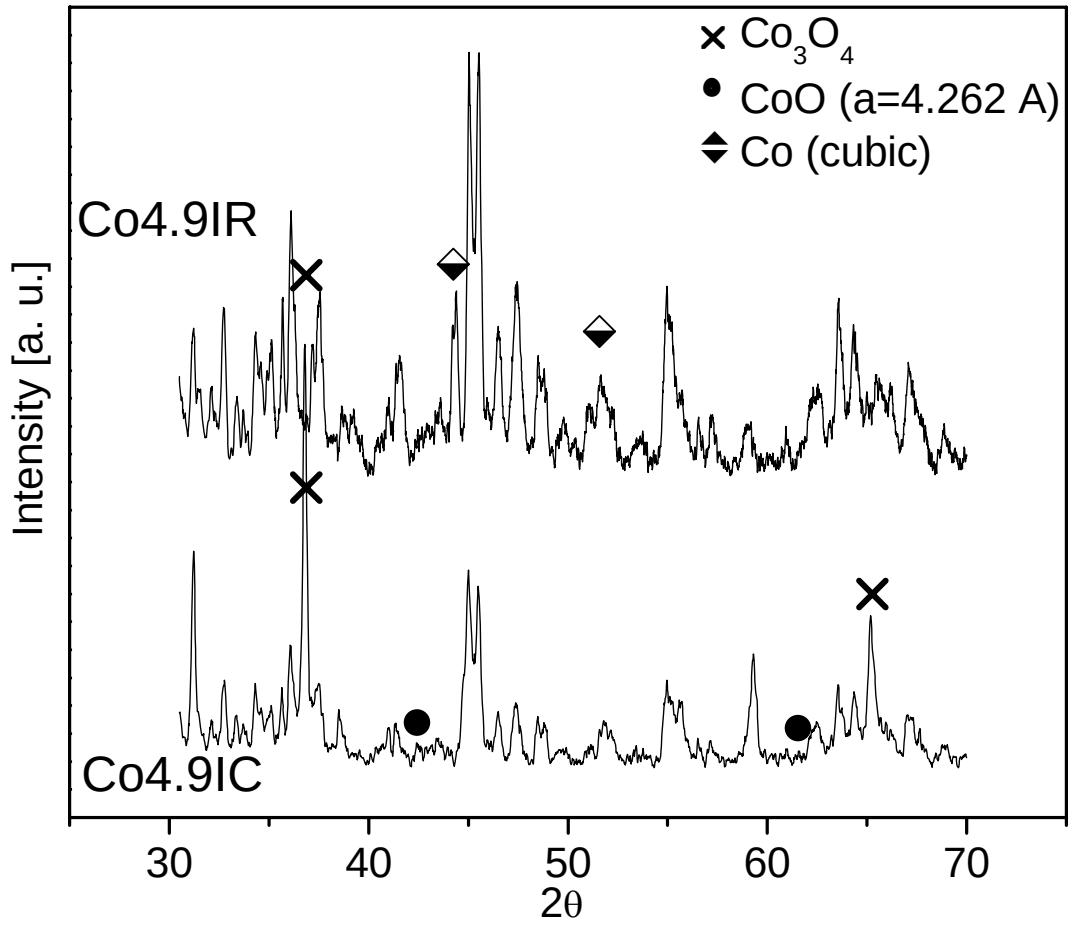
Co3O4
CoO (a=4.262 A)
Co (cubic)
Co4.9IR
Co4.9IC
Intensity [a. u.]
30
40
50
60
70
2θ

Figure 3

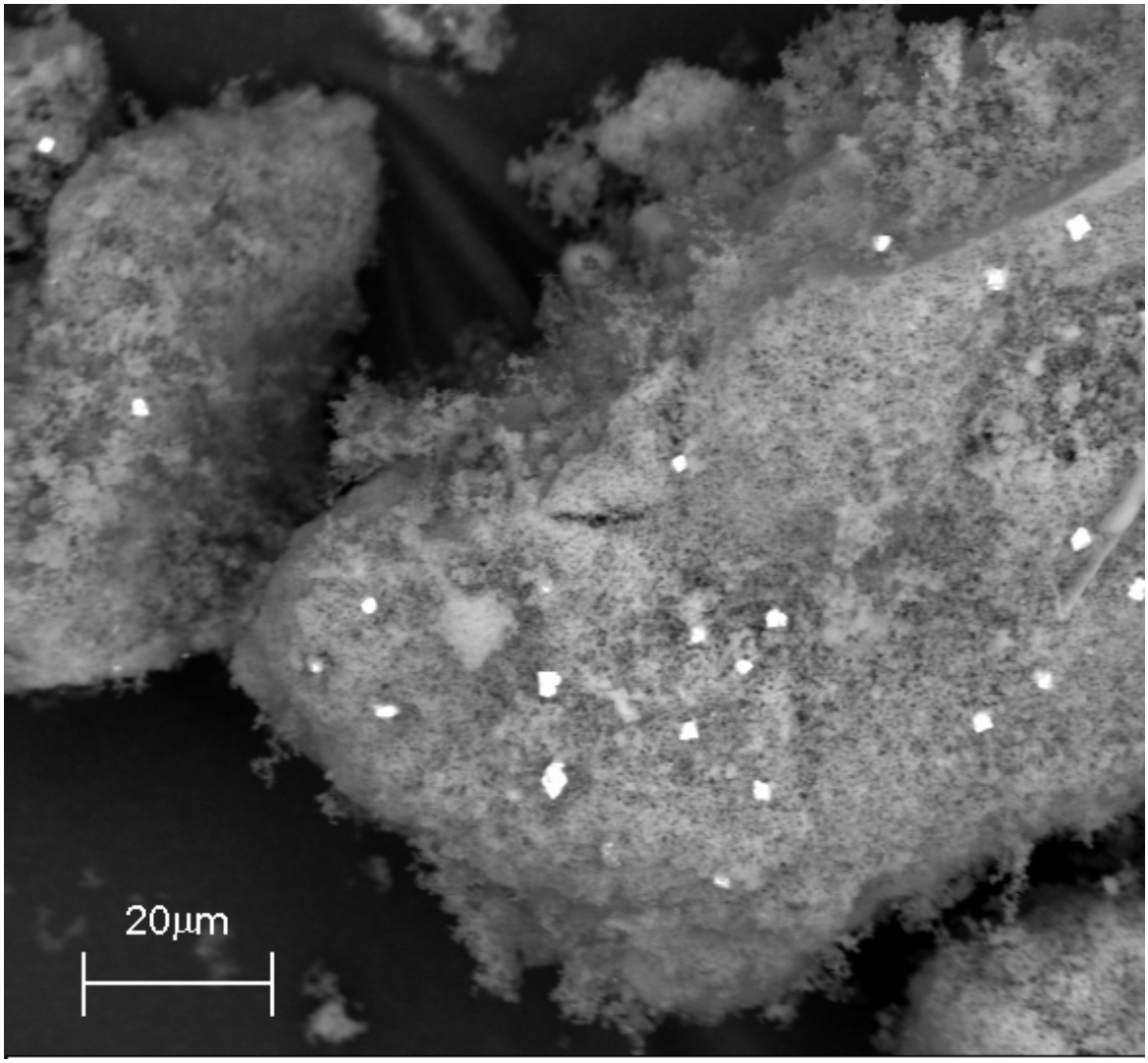

Figure 4:

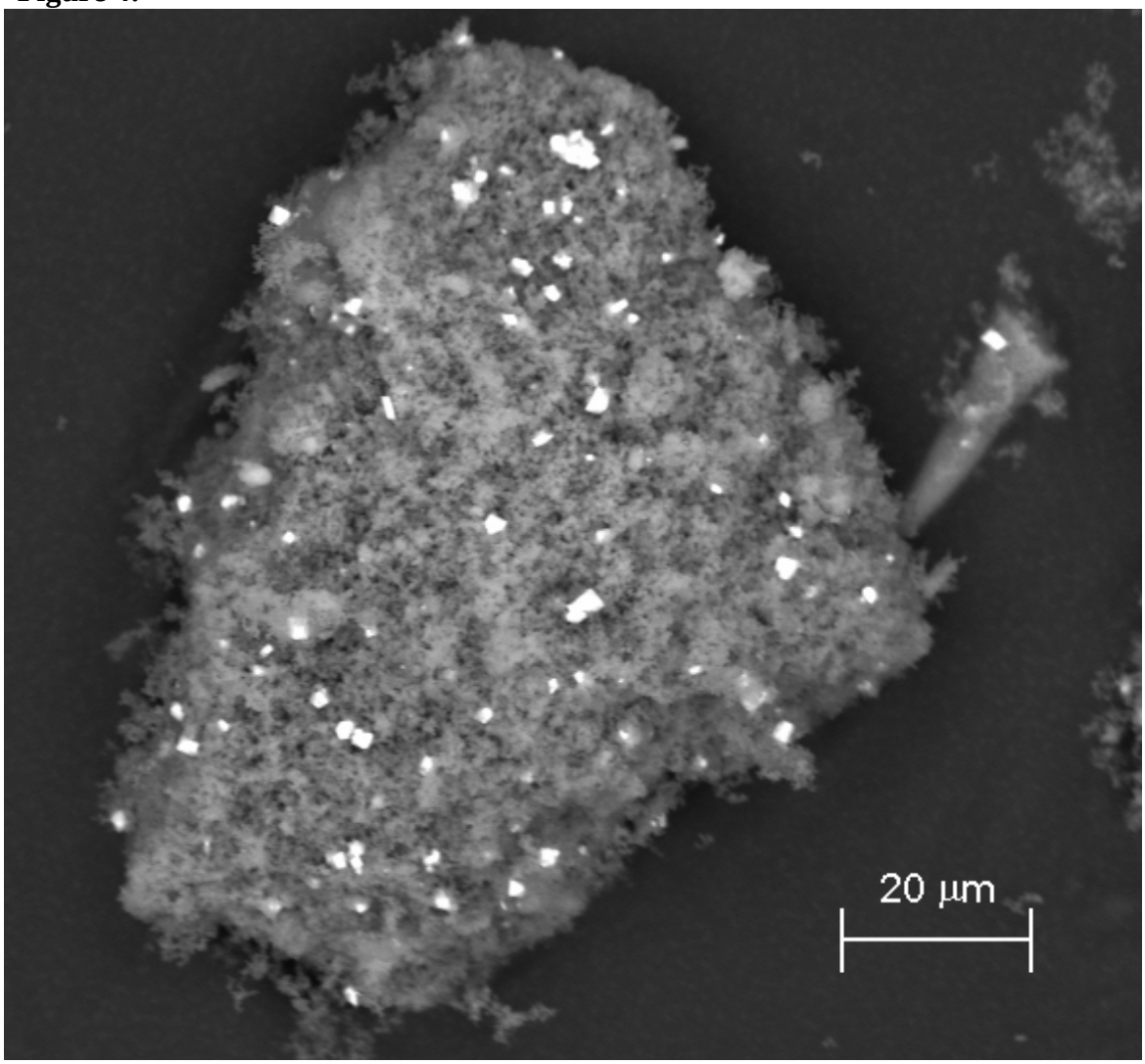

Figure 5:

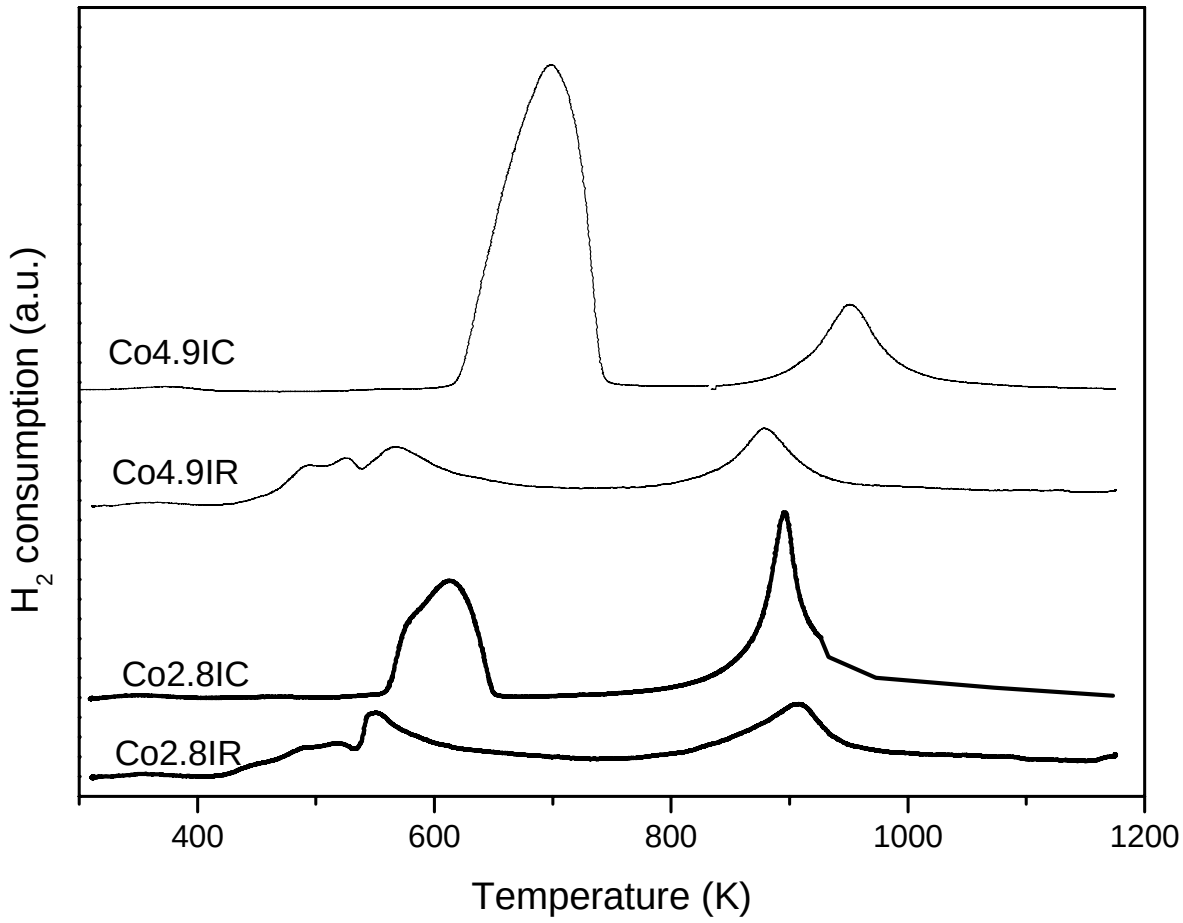
Co4.9IC
Co4.9IR
Co2.8IC
Co2.8IR
H2 consumption (a.u.)
400
600
800
1000
1200
Temperature (K)

Figure 6:

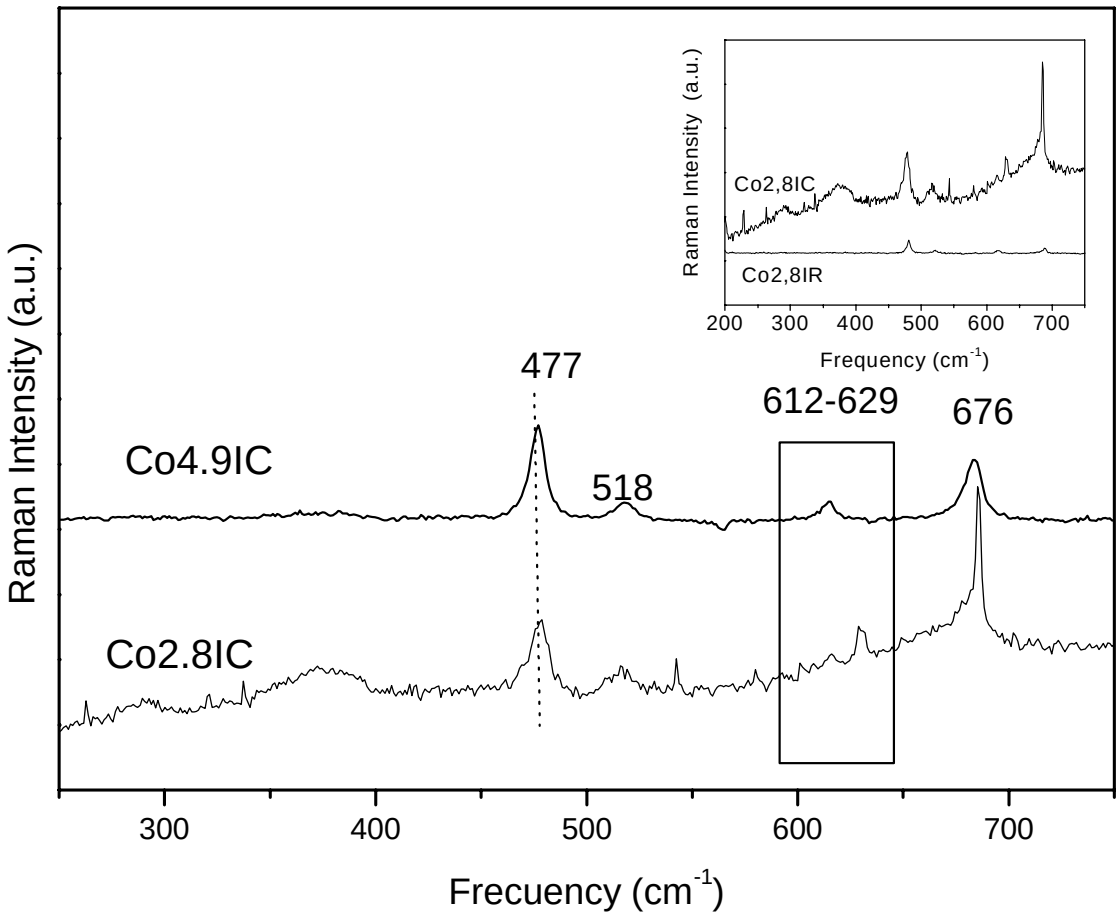
Raman Intensity (a.u.)
Co4.9IC
Co2.8IC
477
518
612-629
676
300
400
500
600
700
Frecuency (cm-1)
Raman Intensity (a.u.)
Co2,8IC
Co2,8IR
200
300
400
500
600
700
Frequency (cm-1)

Figure 7

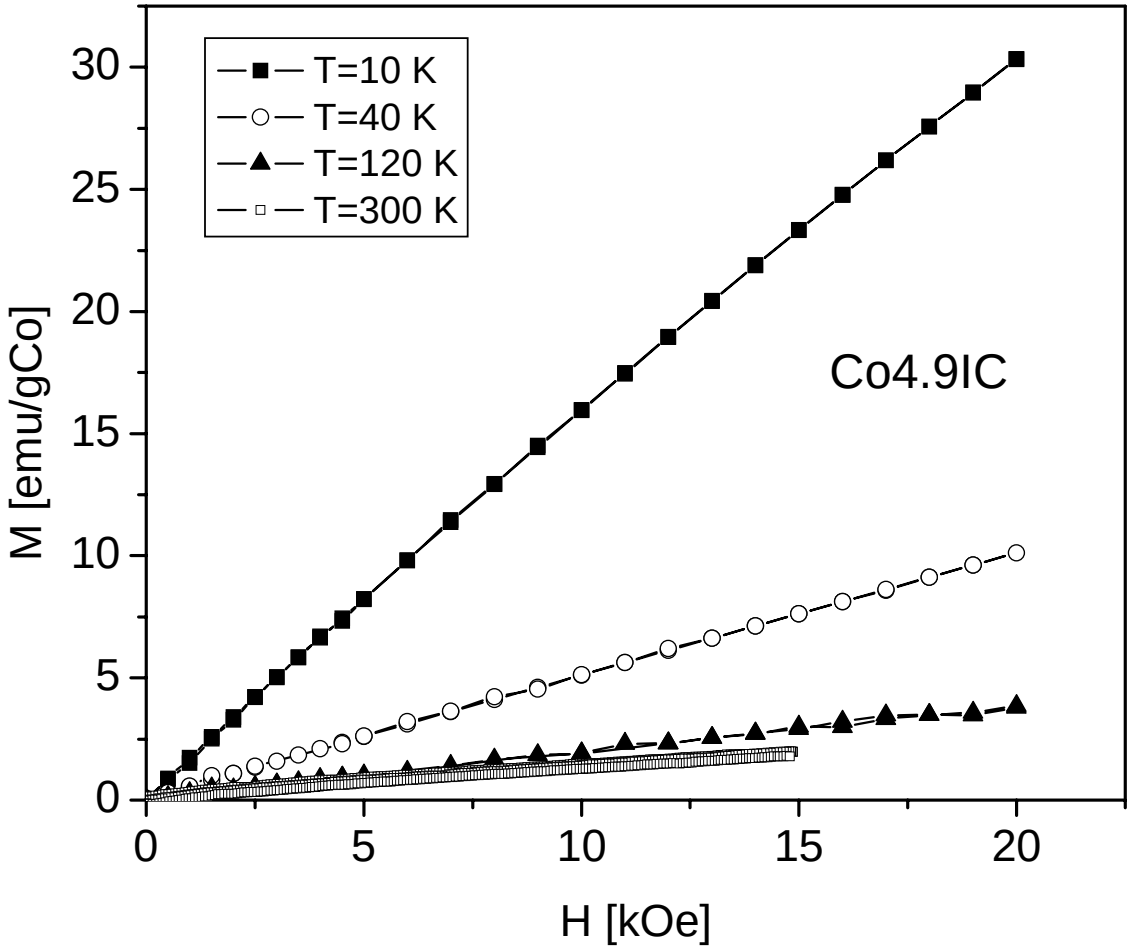

Figure 8

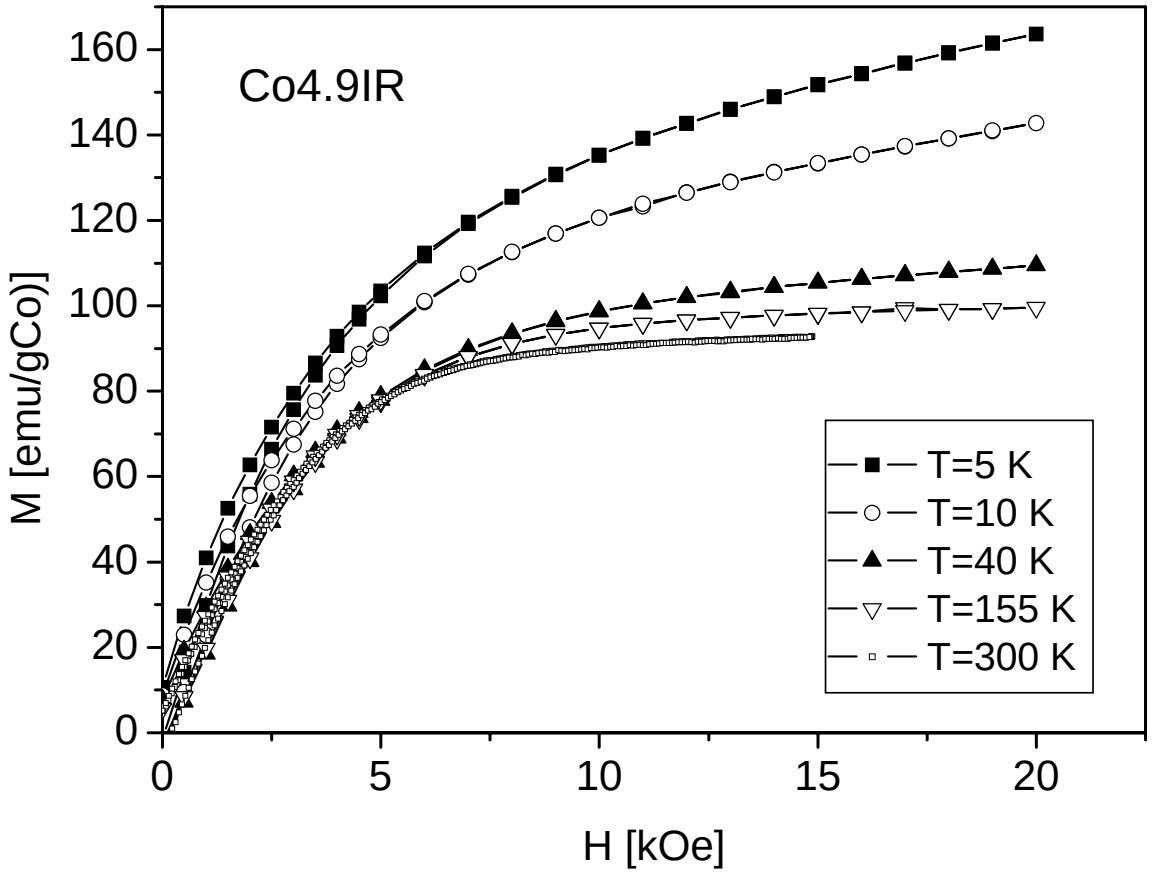
Co4.9IR
M [emu/gCo)]
H [kOe]
0
20
40
60
80
100
120
140
160
0
5
10
15
20
T=5 K
T=10 K
T=40 K
T=155 K
T=300 K